OPEN

Strain induced exciton fine-structure splitting and shift in bent ZnO microwires

Zhi-Min Liao[1]*, Han-Chun Wu[2]*, Qiang Fu[1]*, Xuewen Fu[1], Xinli Zhu[1], Jun Xu[1], Igor V. Shvets[2], Zhuhua Zhang[3], Wanlin Guo[3], Yamin Leprince-Wang[4], Qing Zhao[1], Xiaosong Wu[1] & Da-Peng Yu[1]

[1]State Key Laboratory for Mesoscopic Physics, Department of Physics, Peking University, Beijing 100871, P.R. China, [2]CRANN and School of Physics, Trinity College Dublin, Dublin 2, Ireland, [3]Institute of Nano Science, Nanjing University of Aeronautics and Astronautics, Nanjing 210016, P. R. China, [4]Laboratoire de Physique des Materiaux Divises et Interfaces, CNRS- FRE3300, Universite Paris-Est, Marne la Vallee 77454, France.

Lattice strain is a useful and economic way to tune the device performance and is commonly present in nanostructures. Here, we investigated for the first time the exciton spectra evolution in bent ZnO microwires along the radial direction via high spatial/energy resolution cathodeluminescence spectroscopy at 5.5 K. Our experiments show that the exciton peak splits into multi fine peaks towards the compressive part while retains one peak in the tensile part and the emission peak displays a continuous blue-shift from tensile to compressive edges. In combination with first-principles calculations, we show that the observed NBE emission splitting is due to the valence band splitting and the absence of peak splitting in the tensile part maybe due to the highly localized holes in the A band and the carrier density distribution across the microwire. Our studies may pave the way to design nanophotonic and electronic devices using bent ZnO nanowires.

Zinc oxide (ZnO), a typical II-VI semiconductor with a wide band gap of 3.3 eV, has recently attracted a great deal of attention due to its great potential applications in optoelectronics and piezoelectric devices[1-4]. As an archetype material for the new emerging field called nanopiezotronics, bent ZnO nano/micro wires have also aroused considerable attention and present tremendous opportunities for testing our understanding of condensed matter physics and application-driven research with lattice strain continuously tuned from tensile to compressive across its diameter[5-12]. Recently, a huge number of experimental and theoretical studies have been devoted to understanding the band structure, optical properties, and novel behavior of bent ZnO nano/micro wires. Han et al. observed a bending induced red-shift trend in cathodeluminescence (CL) measurements along the axial direction and attributed their observations to electronic-mechanical coupling[6]. Yan et al. observed a similar red-shift while they explained their results based on the suppression of the phonon-exciton coupling[10]. Despite enormous efforts aimed at understanding the valence band of ZnO and tailoring its properties through strain, the effects of strain on band structure and optical properties have not been clearly interpreted yet. In particular, the nature of the fine structure of the valence-band maximum in ZnO is still under debate after more than half a century's discussion[13]. On the other hand, lattice strain is commonly present in nanostructures during preparation and is a useful and economic way to tune the device performance by modulating the band structure[14,15]. Few reports so far have been focused on the fine structure or the band structure evolution as a function of local strain in nanoscale. Therefore, it is highly important to investigate the exciton spectra and electronic band structure evolution as a function of nanoscale local strain in bent ZnO microwires along the radial direction.

In this study, we demonstrate for the first time the exciton spectra evolution with the continuously tuned lattice strain along the radial direction of bending ZnO microwires using high spatial and energy-resolution CL measurements at 5.5 K, which allow us to divide the curved ZnO microwire into tens of nanoscale sections across its diameter and point by point probe the local exciton spectra along a series of radial cross-sections. The near-band-edge (NBE) emission displays a continuous blue-shift as the CL spectra were collected gradually from the tensile to compressive part. Interestingly, the NBE peak splits into multi fine peaks towards the compressive part while remains one emission peak in the tensile part. In combination with first-principles calculations, we show that the observed NBE emission splitting is due to the valence band (A, B and C band) splitting and the absence of peak splitting in the tensile part maybe due to the highly localized holes in the A band and the carrier density distribution across the microwire. We further show that the observed blue-shift is due to C band evolution

and the corresponding deformation potential $\partial E/\partial \varepsilon_C$ (the slope of the band energy (E) *vs.* the uniaxial strain (ε_c)) was achieved.
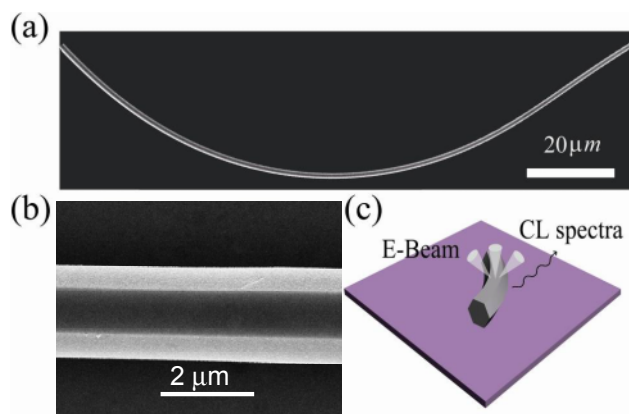
Results

ZnO microwires were synthesized via a chemical vapor deposition method reported elsewhere[16]. The ZnO microwires were dispersed onto a silicon wafer coated with a thin film of Au (10 nm)/Ti (40 nm) and bent with the help of the glass tip under an optical microscope. It is noted that such a bending deformation is elastic because the bent wire will relax to its original straight form after release of the fixed ends. Figure 1(a) shows a representative scanning electron microscope (SEM) image of a bent ZnO microwire with a diameter (defined as the long diagonal of hexagon) of 1.32 μm grown along the direction of [0001], which can be verified by the hexagonal structure shown in Figure 1(b). It is worth noting that the bending stress varies along the axial length of the wire. The straight positions near the two fixed ends are nearly strain-free. As the radius of curvature decreases, the stress increases accordingly. At a given cross-section of the bent part, the outer part is under tensile strain and the inner part under compressive strain along the radial direction, and such a continuous tensile to compressive strain distribution along its diameter is ideal to address the evolution of the electronic band structure with varying strain.
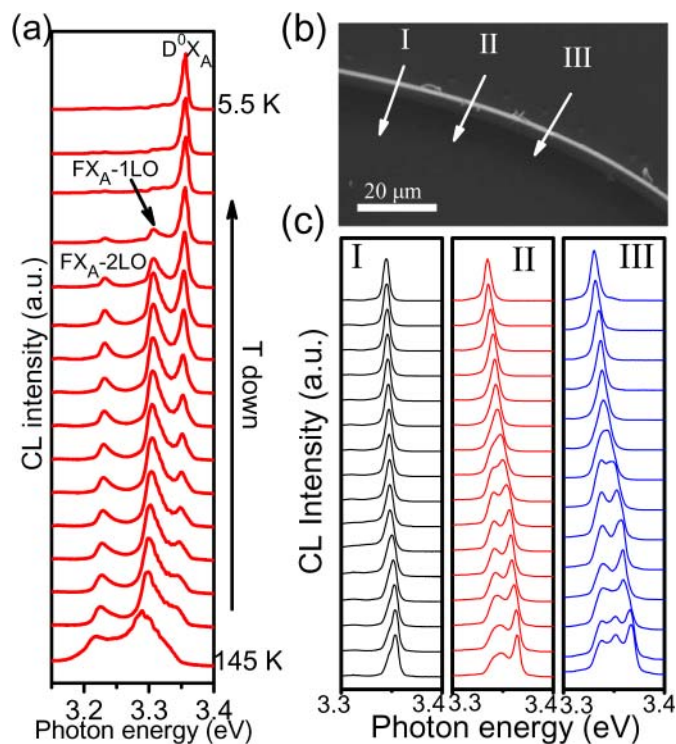
To study the evolution of NBE emission with the local strain distribution, series of CL spectra at liquid helium temperature were collected step by step along the radial direction across the diameter of the ZnO wires at interesting cross-sections with scan step size ~100 nm, as illustrated in the schematic presentation in Figure 1(c). The scan step size of 100 nm is chosen for the consideration of both the interaction volume of the incident electron beam and the exciton diffusion length in ZnO. An electron beam accelerated at 10 kV voltage was used to achieve the optimum spatial resolution with the best signal-to-noise ratio, which results in the effective interaction region of electron beam in ZnO being ~100 nm (with 90% power in this interaction volume, as supported by Monte Carlo simulation[17]). As the exciton diffusion length in ZnO at low temperatures is ~100 nm[18], the exciton emission peaks can clearly reveal the evolution of the band structure with strain by using scan step of ~100 nm.

To accurately compare and identify the NBE emission peaks, the evolution of CL spectra with temperature was analyzed in a strain-free microwire as a reference, as shown in Figure 2(a). At ~145 K, two peaks at 3.295 eV and 3.223 eV are clearly observed, which can

be assigned to first-order longitudinal-optical (LO) phonon replicas of free-excitons (FX_A) (FX_A-1LO) and second-order LO-phonon replicas of FX_A (FX_A-2LO), respectively[19]. As the temperature is reduced, the positions of FX_A-1LO and FX_A-2LO show a blue-shift to higher energies, which is consistent with the increase of band-gap in ZnO with decreasing temperature following the Varshni formula[20]. Moreover, the CL intensity of the donor-bound exciton emission decreases with increasing temperature due to the thermal dissociation. At 145 K, the donor-bound exciton emission peak is mixed with the FX_A-LO peak and can not be distinguished. The absent of FX_A peak and the dominant FX_A-LO peak can be attributed to the strong exciton-phonon interactions caused by surface defects, which have been reported in ZnO film with rough surface[21]. As the temperature is decreased to ~5.5 K, only one emission peak is dominant which becomes increasingly sharp (~9 meV in full width at half maximum (FWHM)) with the energy centered around 3.362 eV, corresponding to the bounded exciton A (D^0X_A)[19]. The detailed NBE peaks of the ZnO wire at ~50 K and ~5.5 K are shown in the Supporting Information Figures S1 and S2 with logarithmic y-axis, respectively. It is recently shown by M. Grundmann *et al.* that ZnO microwires exhibit bulk-like properties with very narrow exciton emission linewidths (<1 meV)[22]. Here, the observed large FWHM of D^0X_A can be understood as following. As shown in Fig. S3, the D^0X_A peak has several shoulders. Through multi-peaks fitting to this peak, at least four peaks were obtained. These closed transition lines may cause the peak broadening. Moreover, possible residual strain in our straight microwire may also broaden the D^0X_A peak.

Figure 2 | **Temperature dependent CL spectra of strain-free ZnO microwire and line scan CL spectra in bent ZnO microwires along the radial direction.** (a) Temperature dependent CL spectra of strain-free ZnO microwire from 145 K to 5.5 K. (b) SEM image of a bent ZnO microwire for CL line scan. The white arrows indicate the positions and the line scan directions for CL measurements. (c) Line scan CL spectra obtained from positions indicated by white arrows in (b). From top to bottom the individual CL spectrums were obtained point by point along the radial directions across the bent ZnO microwire from tensile to compressive edges.

Figure 1 | **Schematic setup and SEM image of the ZnO microwire.** (a) SEM image of an elastically bent ZnO microwire. The two ends are strain-free, and the stress increases with the decrease of the bending curvature radius. (b) SEM image shows the hexagonal structure of the ZnO microwire. (c) The schematic presentation of CL line scan across the cross section of a bent microwire.

Systematic CL spectra were investigated at 5.5 K point-by-point at several radial cross-sections of the bent ZnO microwires. Figure 2(b) indicates 3 representative radial cross-section positions marked "I" to "III" with white arrow lines in the bent microwire, each position with a different bending curvature radius. Figure 2(c) shows individual CL spectra taken from the wire in the three locations indicated by the white arrows in Figure 2(b). The arrangement from the top to bottom corresponds to point-by-point CL measurements from the tensile to compressive edges in step of 100 nm. Along the radial cross-section marked "I" with very small strain, only one intensive peak (FWHM ~9 meV) is observed. Although the peak broadens a little (~3 meV) in the compressive part, no splitting of NBE emission peak can be observed. Interestingly, along the position "II" with larger strain, the NBE emissions still exhibit one intensive peak in the tensile part and show an obvious blue shift from the outer side to the core (from tensile to neutral part) of the ZnO microwire. Moreover, the NBE emission splits into two distinct peaks and shows a significant and continuous blue shift with increasing deformation towards the compressive side. Along the most bent position "III", the emission peak further splits into three fine peaks towards the compressive part (the peaks plotted with logarithmic y-axis are shown in Figure S4), and shows the largest blue shift ~29 meV compared to the core position. Figure 3(a) shows the 3-dimensional presentation of the CL spectra as functions of the photon energy and the positions along the diameter cross-section (at position III) relative to the core of the bent ZnO microwire. It was shown recently that uniaxial tensile and compressive strains were symmetrically distributed with respect to the neutral mid-plane in a bent ZnO microwire[7]. Thus, we can plot the energy position evolution of the three excitonic peaks as a function of strain in Figure 3(b). The strain value ε along the radial direction for a given cross

section of the bent microwire is determined by $\varepsilon = r\kappa$, where r is the radial distance apart from the middle-plane of the cross-section, κ is the local curvature at the cross section of the bent ZnO wire. Figures 3(a) and 3(b) clearly demonstrate that engineering the lattice strain is an effective way to control the optical properties and electronic structure of ZnO. Tens of bent ZnO microwires were studied and similar experimental results were observed (See Supporting Information Figures S5–S8).

In order to determine the dissociation energy of the observed excitons, temperature dependent CL measurements were performed at two different positions with a compressive strain of −0.7% for a bent ZnO microwire. Figure 3(c) shows the temperature dependent CL spectra. One can see from Figure 3(c) that there are two peaks (marked as D^0X_A and D^0X_B) with an energy difference around 15 meV at low temperature. The CL intensity of D^0X_A and D^0X_B decrease with increasing temperature and disappear at temperature above 80 K and 100 K respectively. Interestingly, their peak positions are almost temperature independent which may suggest that the exciton peak position for bent microwire is mainly dominated by the bent strain, thus may benefit the devices based on the bent microwire. Figure 3(d) shows the integrated intensity for D^0X_A and D^0X_B as a function of 1/T. The activation energy (E_T) for D^0X_A and D^0X_B can be obtained by fitting the curves with $I(T) = I_0/[1 + C exp(-E_T/k_BT)]$, where I_0 is the emission intensity at 0 K, C is a constant, and k_B is Boltzmann constant. The fitting results (solid lines in Fig. 3(d)) give E_T as 7 meV and 8.6 meV for D^0X_A and D^0X_B, respectively, corresponding to the thermal energies of 81 K and 100 K. One can clearly see that the activation energy difference (1.6 meV) for D^0X_A and D^0X_B is significantly smaller than their peak splitting (15 meV) which indicates that the NBE emission splitting is not due to the additional donor-bound excitons which involves the holes from the same valence band. Thus, their
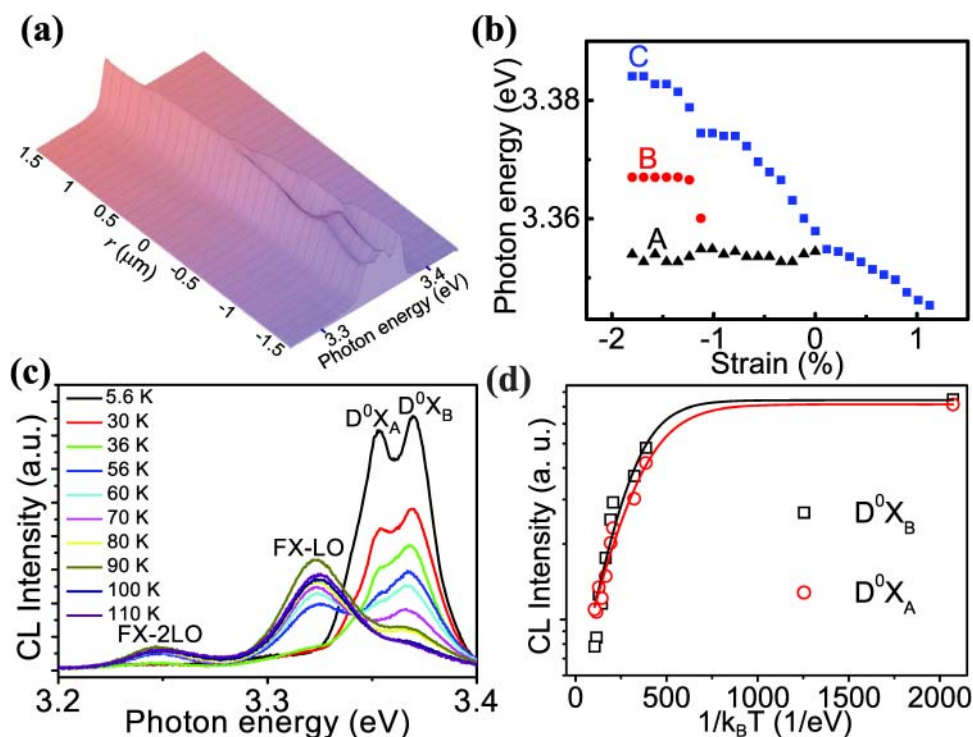
Figure 3 | Emission photon energy as a function of strain and temperature dependent CL spectra of a bent ZnO microwire. (a) The 3-D curves of the relationship between NBE peaks and radial positions (strain) as well as the photon energy, which shows the evolution of the peak position and FWHM more clearly. It is another kind of presentation of that shown in Fig. 2(c) III. (b) The emission photon energy extracted from the center of the CL peaks as a function of strain. (c) Temperature dependent CL spectra of a bent ZnO microwire. (d) Respective integrated intensity for D^0X_A and D^0X_B as a function of 1/T.

transitions involve the holes from two valence bands and the energy separation between excitions reflects the energy separation between respective valence bands.

In order to understand the observed CL spectra under different bending deformations, we have calculated the band structures with varying uniaxial tensile/compressive strain ε_c along the c axis for bulk ZnO as the ground exciton states have the same ordering as the top valence band[13]. Figure 4 (a) shows the band structures for an ideal bulk ZnO without strain from the LDA+U calculations. One can see from the inset in Figure 4 (a) that there are three exciton series derived from a Zn $4s$-like conduction band and O $2p$-like valence bands and are labeled A, B, and C from the top to the bottom, regardless of their symmetry character. Each band is twofold degenerate at Γ point. The band splitting between the A–B exciton and the B–C exciton are 11 meV and 9 meV respectively. Figure 4 (b) summarizes the simulated band gaps corresponding to the A, B, and C bands as a function of strain, where the positive ε_c refers to uniaxial extension along the c axis and the negative one corresponds to uniaxial compression. One can clearly see that the valence band splitting crucially depends on the strain levels and our simple bulk simulations are in reasonable agreement with the experimental observations presented in Figure 3(b). In the strain range from 0 to 0.5 %, A, B, and C bands are close to each other. According to the simulations, at zero stain, the energy splitting between A–B bands is larger than the resolution of the system. However no splitting of NBE emission peak has been observed. Peak broadening due to bent strain and the weak emission from B excitons may impede a clear distinction

between A–B bands. The splitting of the A–B and B–C bands increase as the strain decreases to negative values. When the splitting between the A–B bands is distinguishable, two peaks can be seen from the CL measurements. Further decreasing the negative strain, the band splitting between the B–C bands is large enough to distinguish and three peaks appear in the CL spectra. Moreover, the deformation potential of $\partial E_C/\partial \varepsilon_C$ calculated from the slope of the curve of the energy of C band vs. the uniaxial strain (ε_c) is -1.6 eV from our theoretical simulations, which is between the values obtained from our experiments $\partial E_C/\partial \varepsilon_C$ (-1.46 eV) and Dietrich's experiments $\partial E_A/\partial \varepsilon_C$ (-2.0 eV)[7]. We would like to point out that in our LDA+U simulations, the bandwidth for the valence band is around 4.8 eV which is 10% smaller than the experimental value (5.3 eV)[23]. The difference between the experiment and calculations can be reduced with LDA+GW method[24,25]. We also performed calculations for a ZnO nanowire with a diameter of 0.97 nm (See Figure S10). Similar results have been obtained which suggests the feasibility to design nanophotonic and electronic devices using bent ZnO nanowires.

By calculating the effective mass of holes in the valence bands and considering its continuous variation with varying strain, we can identify the band evolution from compressive to tensile strain. There is a crossover for the three valence bands under tensile strain, as shown in Figure 4(b). As the strain is increased towards positive values, the B band becomes the top band, which agrees well with the experimental observation that the emission peaks in the tensile segment are evolved from the C band because the band splitting between
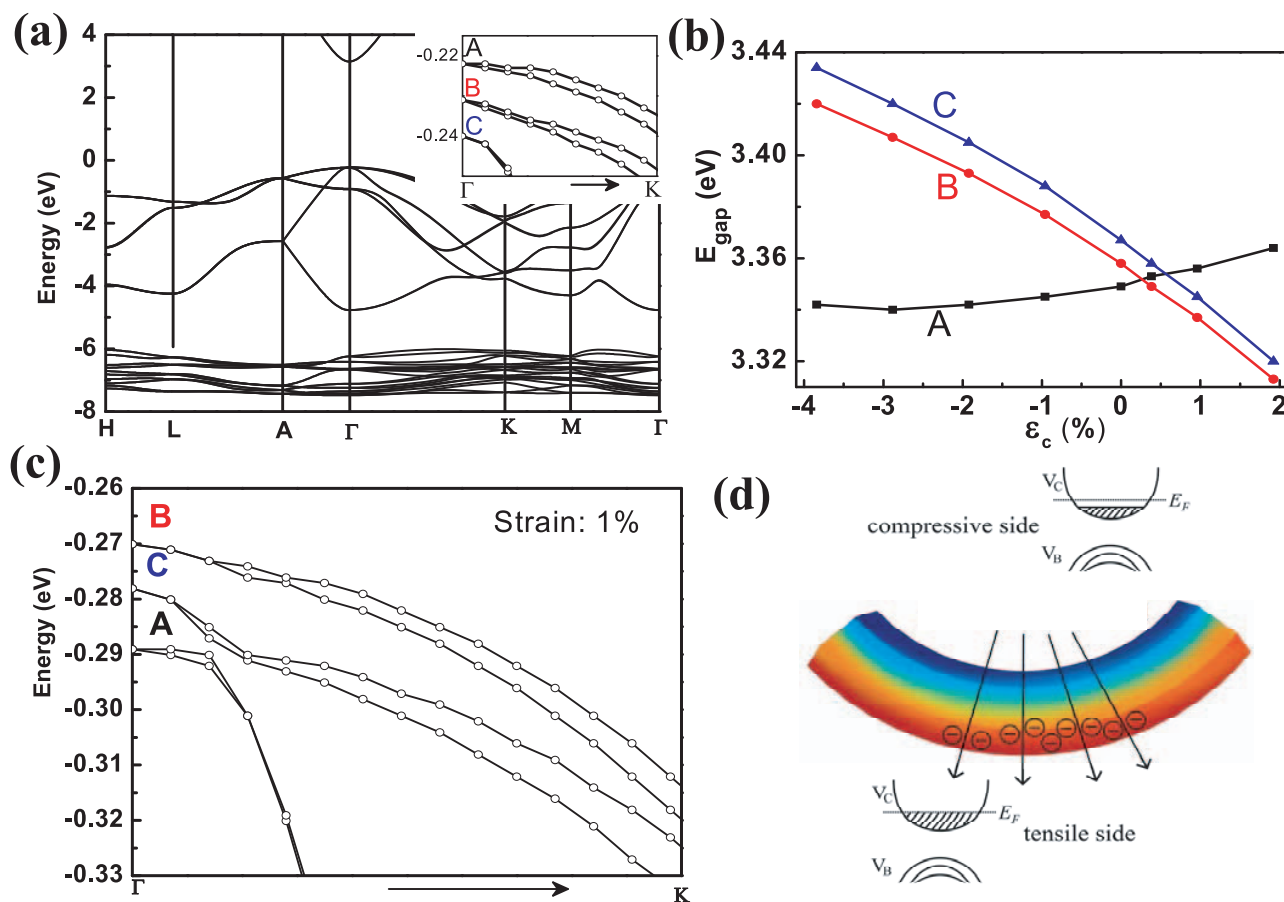
Figure 4 | Simulated band gaps as a function of strain, calculated fine structures near Γ point in ZnO with 1% tensile strain and schematic carrier density distribution across the microwire. (a) Calculated band structures for ideal bulk ZnO without strain from the LDA+U calculations. To compare with the experiments, all calculated conduction bands were shifted up 1.921 eV. Inset: magnifying the fine structures at the top of the valence bands. (b) The simulated band gaps corresponding to the A, B, and C bands as a function of strain. (c) The calculated fine structures at the top of valence bands near Γ point in ZnO with 1% tensile strain. (d) Schematic carrier density distribution across the microwire.

the B–C bands cannot be resolved from CL measurements, as clearly shown in Figures 2(c), 3(a) and 3(b). The theoretical calculations also show that the E_{A-C} also increases with increasing tensile strains for strain larger than 0.5%; however, no emission peak splitting was observed experimentally in the tensile segment. As shown in Figure 4(c), the heavy-hole band (A band) is below the B and C bands under 1% tensile strain and there is a very flat curvature at the top of the A band near Γ point. Therefore, the holes in the A band are less mobile and the efficiency of generating a D^0X_A exciton between the A band and conduction band is very small, which may result in only one emission peak observed in the tensile part. Furthermore, one can see from Figure 4(b) that the band gap of ZnO decrease with increasing tensile strain while the band gap is almost constant in the compressive part. Thus, for a bent ZnO microwire, electrons density will be high in the tensile side, as shown in Figure 4(d). Under the excitation by electron beam, the electron concentration in the tensile part of the ZnO wire will be extremely high and the Fermi level may be lifted into the conduction band, as shown in Figure 4(d). In this condition, only the electrons in the top valence band (C band) can be effectively excited into the conduction band under the electron beam excitation and left holes in the C band which may also result in only one emission peak from the electron-hole recombination in tensile part.

Discussion

We have experimentally and theoretically demonstrated that engineering the lattice strain is an effective way to control the optical properties and electronic structure of ZnO. To the best of our knowledge, we investigated for the first time the exciton spectra evolution in bent ZnO microwires along the radial direction via high spatial/energy resolution CL spectroscopy at 5.5 K. Our experimental method allows us to divide the curved ZnO microwire into tens of nanoscale sections across its diameter and point by point probe the local exciton spectra along a series of radial cross-sections. We show that the exciton peak splits into multi fine peaks towards the compressive part while retains one peak in the tensile part and the emission peak displays a continuous blue-shift from tensile to compressive edges.

In combination with first-principles calculations, we show that the observed NBE emission splitting is due to the valence band splitting. Our calculations further show that the highly localized holes in the A band and the carrier density distribution across the microwire may result in the absence of peak splitting in the tensile part. We further clarify that the observed blue shift is due to C band evolution and the corresponding deformation potential $\partial E/\partial\varepsilon_C$ of -1.6 eV was achieved. Our results shed new light on the strain engineering of ZnO materials and may pave the way to design nanophotonic and electronic devices using bent ZnO nanowires.

Methods

Sample preparation. ZnO microwires were synthesized via a chemical vapor deposition method. The ZnO microwires were dispersed onto a silicon wafer coated with a thin film of Au (10 nm)/Ti (40 nm). To bend the ZnO microwires, wires with diameter larger than 1 μm and length up to hundreds of micrometers were chosen and one end of the microwires was firstly fixed to the substrate using silver paste. The other end was manipulated using a glass tip under an optical microscope and then fixed with sliver paste to keep the wire in a curved shape and strained state after removing the glass tip.

Measurements. The CL spectrum measurements were performed in an Environmental Scanning Electron Microscope (FEI Quanta 200) with a Gatan MonoCL3+ system and a liquid helium stage using an accelerating voltage of 10 keV. The slit width can be chosen from 0.01 to 5 mm. Using a 1200 lines/mm grating and the silt width with 0.02 mm, the system has a spectral resolution of 0.05 nm.

First-principles simulation. The band structure calculations were performed using the Vienna *ab initio* simulation package[26]. We employed the projected augmented plane wave method[27] and the valence configurations of $3d^{10}4s^2$ for Zn and $2s^22p^4$ for O were used. The so-called local-density-approximation (LDA) with on-site Coulomb interaction (U) has been used to calculate the electronic structure[28]. For the LDA+U

simulations in this work, we use U = 6.0 eV and J = 0 eV[29,30]. A cut-off energy of 500 eV has been used for geometry optimization and energy calculations. $5\times5\times3$ and $15\times15\times9$ Monkhorst–Pack k-point grids were applied to sample the Brillouin zone for geometry optimization and energy calculations, respectively. We use the lattice parameters $c_0 = 5.20$ Å, $c_0/a_0 = 1.58$ to calculate the electronic structure of ideal bulk ZnO, and the u value obtained from geometry optimization is 0.383. To simulate the effect of uniaxial tensile/compressive strain ε_c along the c axis, we scale the lattice c parameter with $c = c_0 * (1+\varepsilon_c)$ and lattice a parameter is calculated by $a = a_0 * (1-\varepsilon_c * \upsilon)$, where υ is the Poisson's ratio. In present simulations, a Poisson's ratio of 0.417 is used[31,32].

1. Chu, S., Wang *et al*. Electrically pumped waveguide lasing from ZnO nanowires. *Nat. Nanotechnol.* **6**, 506–510 (2011).
2. Huang, M. H. *et al*. Room-Temperature Ultraviolet Nanowire Nanolasers. *Science* **292**, 1897–1899 (2001).
3. Wang, Z. L. & Song, J. H. Piezoelectric Nanogenerators Based on Zinc Oxide Nanowire Arrays. *Science* **312**, 242–246 (2006).
4. Soci, C. *et al*. ZnO Nanowire UV Photodetectors with High Internal Gain. *Nano Lett.* **7**, 1003–1009 (2007).
5. Xu, S., Qin, Y., Xu, C., Wei, Y., Yang, R. & Wang, Z. L. Self-powered nanowire devices. *Nat. Nanotechnol.* **5**, 366–373 (2010).
6. Han, X. B. *et al*. Electronic and Mechanical Coupling in Bent ZnO Nanowires. *Adv. Mater.* **21**, 4937–4941 (2009).
7. Dietrich, C. P. *et al*. Strain distribution in bent ZnO microwires. *Appl. Phys. Lett.* **98**, 031105 (2011).
8. Chen, R., Ye, Q. L., He, T. C., Wu, T. & Sun, H. D. Uniaxial tensile strain and exciton–phonon coupling in bent ZnO nanowires. *Appl. Phys. Lett.* **98**, 241916 (2011).
9. Wang, X. D. *et al*. Piezoelectric Field Effect Transistor and Nanoforce Sensor Based on a Single ZnO Nanowire. *Nano Lett.* **6**, 2768–2772 (2006).
10. Yan, B. *et al*. Localized suppression of longitudinal-optical-phonon–exciton coupling in bent ZnO nanowires. *Nanotechnology* **21**, 445706 (2010).
11. Han, X. B. *et al*. Bending-Induced Conductance Increase in Individual Semiconductor Nanowires and Nanobelts. *Nano Res.* **2**, 553–557 (2009).
12. Xue, H. Z. *et al*. Probing the strain effect on near band edge emission of a curved ZnO nanowire via spatially resolved cathodoluminescence. *Nanotechnology* **21**, 215701 (2010).
13. Lambrecht, W. R. L., Rodina, A. V., Limpijumnong, S., Segau, B. & Meyer, B. K. Valence-band ordering and magneto-optic exciton fine structure in ZnO. *Phys. Rev. B* **65**, 075207 (2002).
14. Newton, M. C., Leake, S. J., Harder, R. & Robinson, I. K. Three-dimensional imaging of strain in a single ZnO nanorod. *Nature Mater.* **9**, 120–124 (2010).
15. Liu, Z., Wu, J., Duan, W., Lagally, M. G. & Liu, F. Electronic Phase Diagram of Single-Element Silicon "Strain" Superlattices. *Phys. Rev. Lett.* **105**, 016802 (2010).
16. Bie, Y. Q. *et al*. Controllable synthesis and characterization of tube brush-like ZnO nanowires produced via a simple chemical vapor deposition method. *Appl. Phys. A* **98**, 491–497 (2010).
17. Xu, J. *et al*. Cathodoluminescence Study of InGaN/GaN Quantum-Well LED Structures Grown on a Si Substrate. *J. Electron. Mater.* **36**, 1144–1147 (2007).
18. Yoo, J., Yi, G. C. & Dang, L. S. Probing exciton diffusion in semiconductors using semiconductor-nanorod quantum structures. *Small* **4**, 467–470 (2008).
19. Özgür, Ü. *et al*. A comprehensive review of ZnO materials and devices. *J. Appl. Phys.* **98**, 041301 (2005).
20. Cao, B. Q., Cai, W. P. & Zeng, H. B. Temperature-dependent shifts of three emission bands for ZnO nanoneedle arrays. *Appl. Phys. Lett.* **88**, 161101 (2006).
21. Hong, W. K., Jo, G., Choe, M., Lee, T., Sohn, J. I. & Welland, M. E. Influence of surface structure on the phonon-assisted emission process in the ZnO nanowires grown on homoepitaxial films. *Appl. Phys. Lett.* **94**, 043103 (2009).
22. Dietrich, C. P. *et al*. Defect properties of ZnO and ZnO:P microwires. *J. Appl. Phys.* **109**, 013712 (2011).
23. Kobayashi, M. *et al*. Experimental observation of bulk band dispersions in the oxide semiconductor ZnO using soft x-ray angle-resolved photoemission spectroscopy. *J. Appl. Phys.* **105**, 122403 (2009).
24. Bechstedt, F., Fuchs, F. & Kresse, G. Ab-initio theory of semiconductor band structures: New developments and progress. *Phys. Status Solidi B* **246**, 1877–1892 (2009).
25. Yan, Q. *et al*. Band parameters and strain effects in ZnO and group-III nitrides. *Semicond. Sci. Technol.* **26**, 014037 (2011).
26. Kresse, G. & Hafner, J. Ab initio molecular dynamics for liquid metals. *Phys. Rev. B* **47**, R558 (1993).
27. Payne, M. C., Teter, M. P., Allan, D. C., Arias, T. A. & Joannopoulos, J. D. Iterative minimization techniques for ab initio total-energy calculations: molecular dynamics and conjugate gradients. *Rev. Mod. Phys.* **64**, 1045 (1992).
28. Bengone, O., Alouani, M., Blöchl, P. E. & Hugel, J. Implementation of the projector augmented-wave LDA+U method: Application to the electronic structure of NiO. *Phys. Rev. B* **62**, 16392 (2000).
29. Dong, C. L. *et al*. Electronic structure of nanostructured ZnO from x-ray absorption and emission spectroscopy and the local density approximation. *Phys. Rev. B* **70**, 195325 (2004).
30. Chun, B. S. *et al*. The effect of deposition power on the electrical properties of Al-doped zinc oxide thin films. *Appl. Phys. Lett.* **97**, 082109 (2010).

31. Kobiakov, I. B. Elastic, piezoelectric and dielectric properties of ZnO and CdS single crystals in a wide range of temperatures. *Solid State Commun.* **35**, 305–310 (1980).

32. Shao, Z. *et al.* Influence of carrier concentration on piezoelectric potential in a bent ZnO nanorod. *J. Appl. Phys.* **108**, 124312 (2010).

Author contributions

D.P.Y. designed the study. Z.M.L., Q.F., X.F., X.Z., and J.X. performed the experiments. H.C.W. carried out the first-principle simulations. Z.M.L. and H.C.W. analyzed the data and wrote the article. All authors contributed to discussion and reviewed the manuscript.

Additional information

Supplementary information accompanies this paper at http://www.nature.com/scientificreports

How to cite this article: Liao, Z. *et al.* Strain induced exciton fine-structure splitting and shift in bent ZnO microwires. *Sci. Rep.* **2**, 452; DOI:10.1038/srep00452 (2012).